ELSEVIER

Physica D 139 (2000) 217–230

PHYSICA D

www.elsevier.com/locate/physd

Identification of symmetry breaking and a bifurcation sequence to chaos in single particle dynamics in magnetic reversals

A. Ynnerman, S.C. Chapman*, M. Tsalas, G. Rowlands

Department of Physics, University of Warwick, Coventry CV4 7AL, UK

Received 3 December 1998; received in revised form 3 May 1999; accepted 12 May 1999
Communicated by J.D. Meiss

Abstract

Regular and stochastic behaviour in single particle orbits in static magnetic reversals have wide application in laboratory and astrophysical plasmas and have been studied extensively. In a simple magnetic reversal of the form $\mathbf{B} = B_0(f(z), 0, b_1)$ with an odd function $f(z)$ providing the reversing field component and a constant b_1 providing linking field component, the system has three degrees of freedom but only two global (exact) constants of the motion, namely the energy, h, and the canonical momentum in the y-axis, P_y. Hence, the system is non-integrable and the particle motion can, under certain conditions, exhibit chaotic behaviour. Here we consider the dynamics when a constant shear field, b_2, is added so that $\mathbf{B} = B_0(f(z), b_2, b_1)$. In this case, the form of the potential changes from quadratic to velocity dependent. We use numerically integrated trajectories to show that the effect of the shear field is to break the symmetry of the system so that the topology of the invariant tori of regular orbits is changed. This has several important consequences: (1) the change in topology cannot be transformed away in the case of $b_2 \neq 0$ and hence the system cannot be transformed back to the more easily understood shear free case ($b_2 = 0$); (2) invariant tori take the form of nested Moebius strips in the presence of the shear field. The route to chaos is via bifurcation (period doubling) of the Moebius strip tori.

PACS: 05.45.+b; 07.05.Rm; 52.65.Cc; 94.30.Ej

Keywords: Magnetic current sheet; Chaos; Bifurcation; Computer visualization

1. Introduction

Considerable literature exists concerning single-particle dynamics in static magnetic reversals where a shear field is absent, particularly for application to the Earth's geotail, e.g. [3,8,15] (and references therein). Recently, time dependence has been included, e.g. [5]. Magnetic models of the form $\mathbf{B} = B(f(z), 0, b_1)$ which have no shear

* Corresponding author. Tel: +44-1203-523390.
E-mail address: sandrac@astro.warwick.ac.uk (S.C. Chapman)

0167-2789/00/$ – see front matter
PII: S0167-2789(99)00144-X

component have the advantage that a Hamiltonian with a quadratic potential exists to describe the dynamics, hence their attraction as an approach to astrophysical problems of interest.

However, observations suggest that a shear field is present in the Earth's geotail, e.g. [13] and bow shock, e.g [9]. The presence of a shear field is also important in magnetic reversals in solar flares, e.g. [12]. This has prompted more recent studies for specific field models; these are indicative that energization and scattering of particles in static reversals is fundamentally different in the presence of a shear field, see e.g. [1,4,11,16]. In this paper, we show how the underlying dynamics in a magnetic reversal with shear component differs from that with zero shear. Although the same exact invariants, and the same number of adiabatic invariants [6] can be shown to exist as in the shear free field case, the Hamiltonian takes a distinctively different form. The dynamics is also characterized by examining numerically integrated trajectories in three-dimensional space as well as by judicious choice of Poincare surfaces of section.

2. System of equations

We will first summarize the properties of single particle motion in a simple magnetic reversal with general z dependence and shear, which is of the form:

$$\mathbf{B} = B_0(f(z), b_2, b_1), \tag{1}$$

where $z = Z/L$ is normalized to a convenient length scale of the system L. This simple model has application in astrophysical plasmas as any convective electric field, $\mathbf{E}$, such that $\mathbf{E} = -\mathbf{u}_\mathrm{T} \times \mathbf{B}$ can be included with a de Hoffman Teller frame transformation with velocity $\mathbf{u}_\mathrm{T}$. Here, we will work in the frame where the electric field is zero. In terms of ideal MHD, where $\mathbf{E} + \mathbf{u} \wedge \mathbf{B} = 0$ and $\mathbf{u}$ is the bulk plasma flow velocity, this is equivalent to moving in the rest frame of the plasma. It is equivalent to the Lorentz transformation of the fields $\mathbf{E}' = \mathbf{E} + \mathbf{v} \wedge \mathbf{B}$, with $\mathbf{E}' = 0$ [2,10]. One can obtain the vector potential, $\mathbf{A}$, from:

$$\mathbf{B} = \nabla \times \mathbf{A} \tag{2}$$

a solution of which is

$$\mathbf{A} = B_0(-\alpha z, b_1 x - F(z), -\beta x), \tag{3}$$

where $\beta - \alpha = b_2$, and $F(z) = \int f(z)\mathrm{d}z$. The Hamiltonian is then

$$H = \frac{1}{2m}(\mathbf{P} - q\mathbf{A})^2 \tag{4}$$

with q and m being the charge and the mass of the particle, respectively. Hamiltons equations are then:

$$\frac{\mathrm{d}x}{\mathrm{d}\tau} = p_x + \alpha z, \tag{5}$$

$$\frac{\mathrm{d}y}{\mathrm{d}\tau} = p_y + F(z) - b_1 x, \tag{6}$$

$$\frac{\mathrm{d}z}{\mathrm{d}\tau} = p_z + \beta x, \tag{7}$$

$$\frac{\mathrm{d}p_x}{\mathrm{d}\tau} = -\beta(p_z + \beta x) + b_1(p_y + F(z) - b_1 x), \tag{8}$$

$$\frac{\mathrm{d}p_y}{\mathrm{d}\tau} = 0, \tag{9}$$

$$\frac{\mathrm{d}p_z}{\mathrm{d}\tau} = -\alpha(p_x + \alpha z) - f(z)(p_y + F(z) - b_1 x), \tag{10}$$

where time has been normalized to $\tau = t\Omega_0$ with $\Omega_0 = qB_0/m$, and the canonical momenta to $\mathbf{p} = \mathbf{P}/qB_0$. p_y is a constant of the motion and we can take it to be equal to zero without loss of generality. Thus, the Hamiltonian takes the form

$$H = \frac{1}{2}(p_x + \alpha z)^2 + \frac{1}{2}(p_z + \beta x)^2 + \frac{1}{2}(F(z) - b_1 x)^2. \tag{11}$$

A further constant appears when we substitute Eqs. (6) and (7) into Eq. (8) and integrate over time. This integration constant is related to p_x, y and z through

$$I = p_x - b_1 y + \beta z. \tag{12}$$

The Poisson bracket of p_y and I is $[p_y, I] = -b_1$ and thus the two constants are in involution only when $b_1 = 0$ in which case I is the third global invariant and the equations of motion can be solved exactly. However, islands of periodic or quasi-periodic orbits can exist even in the non-integrable system when b_1 is not equal to zero. A local constant of the motion must exist in these regions to decouple the x and z motion. In the special case where $b_2 = 0$, [3] identified this constant as

$$J = \oint \dot{z}\,\mathrm{d}z \tag{13}$$

where the integration is over a z-period. In this case $\alpha = \beta = 0$ and the potential takes a quadratic form. The equations of motion remain unchanged under the transformation $z \to -z$ and $\dot{z} \to -\dot{z}$. This symmetry appears geometrically, in that the Poincaré surface of section plots constructed for the $z = 0$ section are identical for the particles going up ($\dot{z} > 0$) and the particles going down ($\dot{z} < 0$). In addition, when $b_2 = 0$, there is an integrable orbit on the $z = 0$ plane, defined by $\mathrm{d}z/\mathrm{d}\tau = 0$ for arbitrary b_1 and $F(z = 0) = 0$. There is no corresponding orbit when b_2 is finite. This suggests that it is not possible to use a transformation to reduce the system back to a shear free problem. Using a multiple timescale perturbation technique, [6] examined the case of a finite b_2 component. An invariant equivalent to Eq. (13) was found and shown to be an approximate constant of the motion, hence regular KAM surfaces still exist in the $b_2 \neq 0$ system.

The full set of Eqs. (5)–(10) can only be solved numerically; hence we investigate the dynamics in the $b_2 \neq 0$ system by numerical integration of the equations of motion in six-dimensional (x, y, z, v_x, v_y, v_z) phase space. The original six-dimensional system can be reduced to four-dimensions by means of its Hamiltonian properties and the isolating integral, p_y, to give Eq. (11). It is then noted that $H = H(x, z, p_x, p_z)$, so that an orbit defined by $H = \text{const}$ will require at most three-dimensions to characterize its dynamics geometrically. We therefore rely on (i) the existence of KAM surfaces and (ii) visualization in three dimensions to examine the dynamics numerically. The latter has required the use of Virtual Reality to obtain a fully three-dimensional display of the trajectories in configuration (x, y, x or equivalently, x, v_x, z) space. Here, we show perspective plots of views of the trajectories in three-dimensions.

3. Numerically integrated orbits

In the numerical treatment of the system, a simple model for the field reversal was used

$$f(z) = \tanh(z). \tag{14}$$

All particles are in the $z = 0$ plane at $t = 0$. There are then three classes of particle orbits (see, e.g. the review by [8]): transient trajectories that transit the reversal once (See Fig. 1(b)), stochastic trajectories (See Fig. 1(c)) that after entry interact with the reversal many times but will ultimately exit the reversal and regular trajectories (See Fig. 1(a)) that remain on KAM surfaces and are trapped indefinitely within the reversal. Hence Eq. (14) has the property that all orbits will at sufficiently large t leave the reversal unless they are regular – allowing regular orbits to be identified numerically.

The numerical integration of the studied orbits in x, y, z, v_x, v_y, v_z space was performed using an adaptive time step, adaptive order, Adams method [7,14].

The trajectories shown were initiated with $y = z = 0$. Phase space could then be explored by varying x to obtain different trajectories in phase space for a given field configuration (b_1, b_2). The initial v_x was chosen to be zero so that the trajectory was initiated on the x-axis and v_y was obtained from Eq. (6) for a given x, so that all orbits have the same $p_y = 0$. To complete the set of initial conditions, v_z was obtained from Eqs. (7) and (11), given a fixed total energy, H.

It is useful to relate each of the trajectories in Fig. 1(a–c) in terms of the corresponding surface of section (SOS) plot in Fig. 1(d). The plot shows the $\dot{x}, x$, coordinates of the trajectories as they intersect the $z = 0$ plane. The initial v_x, v_y and v_z are chosen such that the velocity space (which is constrained to the surface of a sphere by the energy h) is sampled at regular intervals on the SOS plot. Trajectory (a) then corresponds to the stable orbit at the centre of the nested KAM tori at $x = 0.725$. Trajectory (c) intersects the SOS at $x = 0.36$, in a region characterized by stochastic trajectories. Trajectory (b) is also stochastic but exits the region in which the field varies ($z \leq 1$) after a single crossing of the SOS. Trajectories of this kind are "transient" and correspond to the empty regions in the SOS plot; we distinguish these regions by plotting intersections of the $z = 0$ plane on the SOS after several tens of gyroperiods from the start of the trajectory have elapsed, at which time transient orbits have ceased to intersect $z = 0$ (see [8]).

4. Bifurcation sequence

The principal effect of finite b_2, is that, unlike the $b_2 = 0$ system, for certain values of b_2 regular orbits are absent [6]. Here we characterize the transition between these regions of global chaos and regions exhibiting regular orbits by the topology of the corresponding 3D trajectories. We start with the limiting case of a large b_2. In the $b_2 \to \infty$ limit, the system is integrable and the dominating trajectory is simply the circular motion around the strong b_2 field aligned with the y-axis, see Fig. 2(a). The view of the same trajectory along the x-axis, Fig. 2(b), reveals the effect of the x and z components of the magnetic field, which are distorting the circular orbit. In this projection, it is observed that the distortion is in the shape of the figure of eight. In Fig. 2(c) the corresponding SOS plot is shown. At large b_2, phase space is dominated by simple KAM surfaces. As the value of b_2 is reduced, the distortion of the central orbit increases and at $b_2 \approx 0.188$, the system bifurcates. This is shown in Fig. 3, which is a zoom of the SOS in the region of the period 2 orbit at the centre of the nested KAM tori. From the SOS, we see that as b_2 is decreased by 1 part in 10^2, the innermost KAM tori bifurcate successively. The first bifurcation can only be resolved adequately on SOS plots. Through repeated bifurcations, the system enters a chaotic interval in b_2 for which no stable periodic orbits are found as shown in the SOS plot in Fig. 4. In three-dimensions, we can isolate the central periodic orbit and numerically identify three successive bifurcations. These are shown in Fig. 5. The position of the central orbit for the sequence as a function of b_2 is shown in Fig. 6. Figs. 5(d) and (c) then correspond to the central KAM surface (periodic orbit) in SOS; Figs. 3(d) and (c), respectively.

In the interval of approximately $0.178 \leq b_2 \leq 0.007$, no stable periodic orbits are found in the system. An example for one value of b_2 is shown in Fig. 4; an SOS plot demonstrating the absence of regular trajectories for this interval.

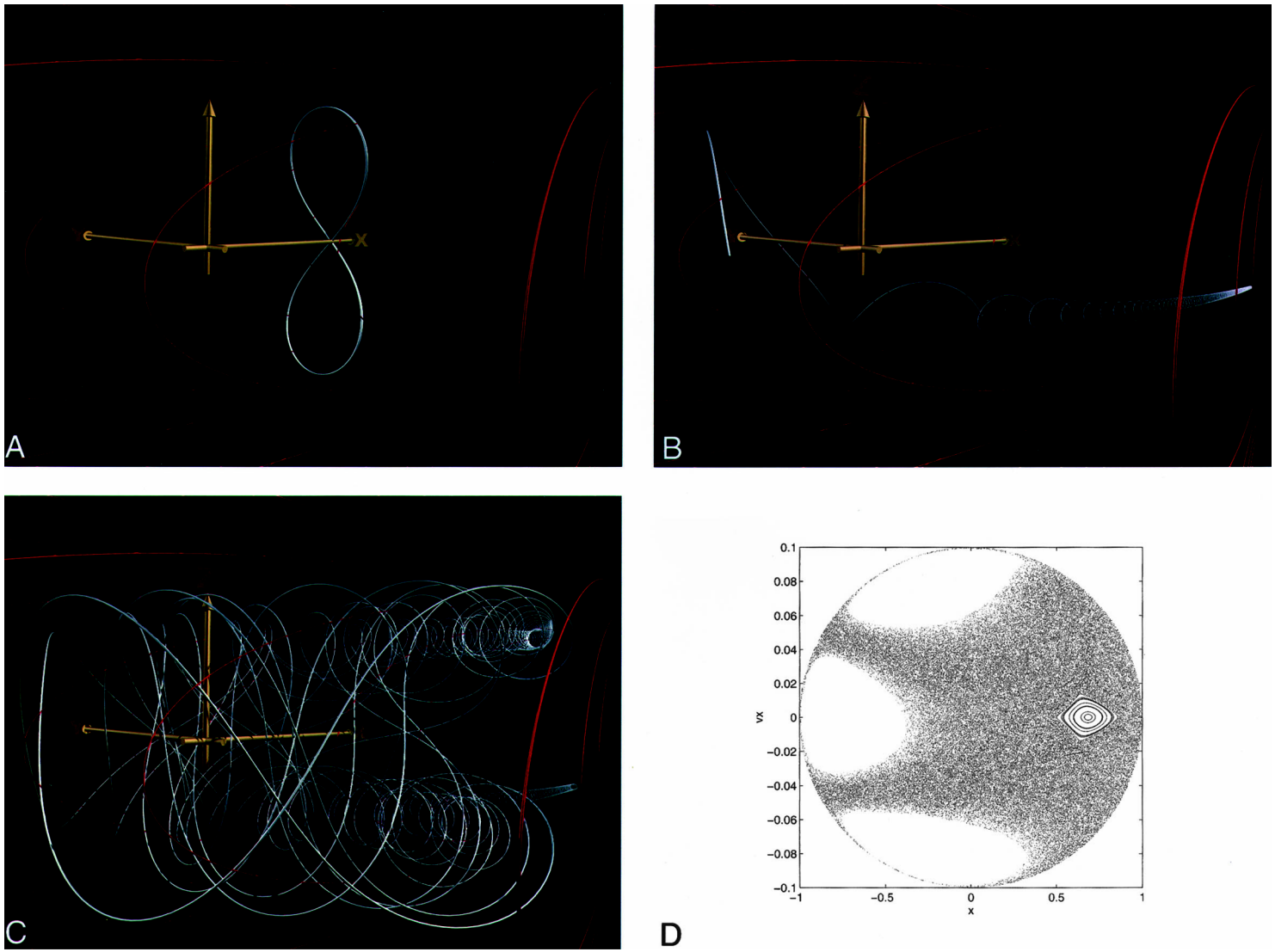

Fig. 1. The three types of particle trajectories in three-dimensional configuration space for $b_2 = 0$. In this and all configuration space plots to follow, the x, y, z (or x, v_x, z) axes are coloured red, blue and green, respectively. The red curved lines indicate the magnetic field lines. In (a) an example of a regular trapped particle trajectory is shown. The initial value of x is 0.725, compare the SOS plot in (d). In (b) a transient trajectory corresponding to $x = -0.38$ is shown. The particle only traverses the reversal once and then escapes to infinity. In (c) an example of a stochastic particle trajectory is given. The particle stays in the reversal for a significantly longer time than a transient particle and exhibits chaotic motion as it is traversing the reversal several times, but eventually escapes to infinity. The trajectory corresponds to $x = 0.35$. The dotted grey lines indicate the magnetic field lines in the reversal. In (d) the SOS plot for $b_2 = 0$ is shown.

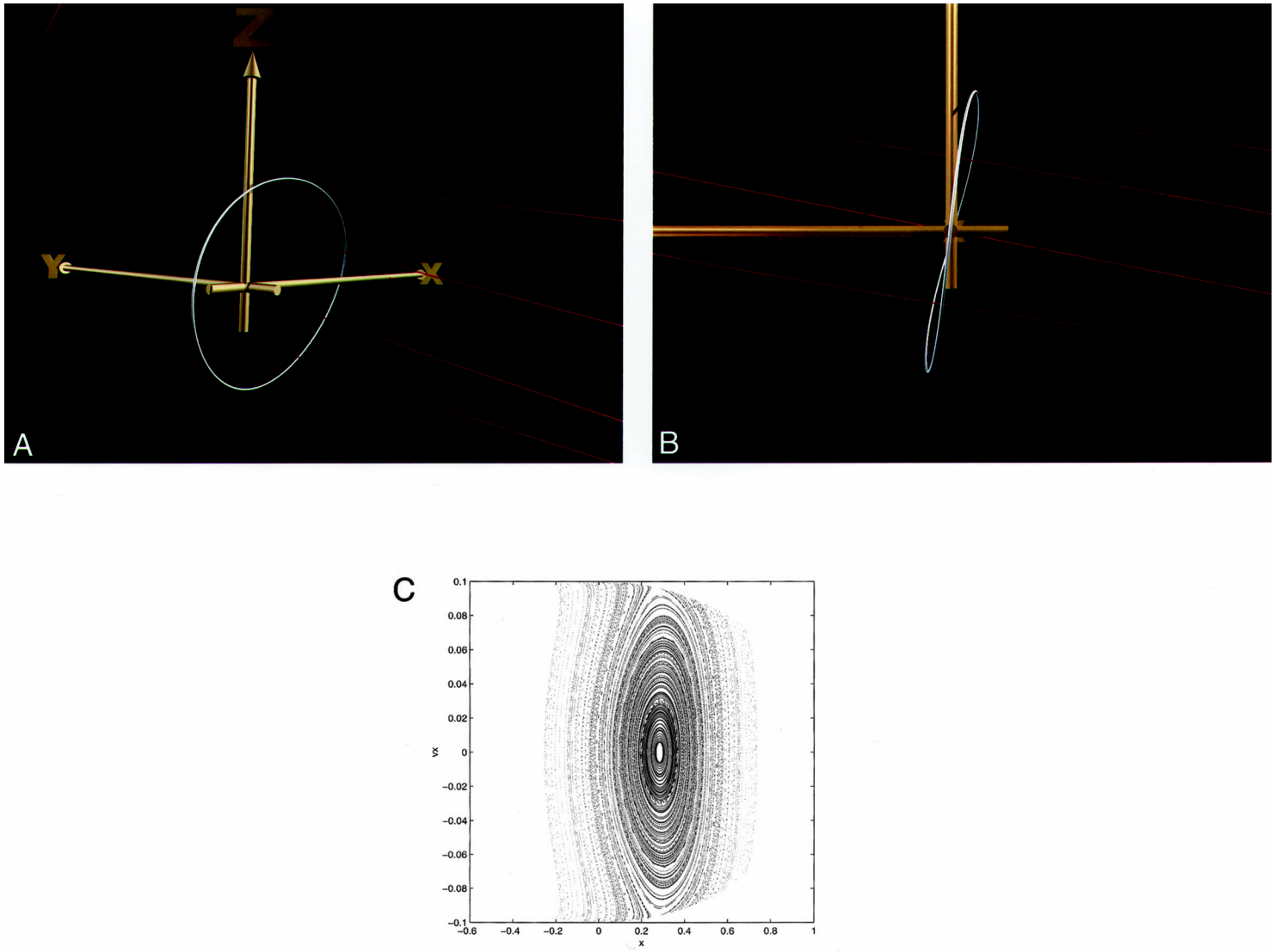

Fig. 2. Trajectory in three-dimensional configuration space (a,b) is shown for $b_2 = 5 \times b_1$. The view in (b) is along the x-axis. The distortion of the circular orbit appears, in this perspective, as the figure of eight. In (c) the corresponding SOS plot is shown.

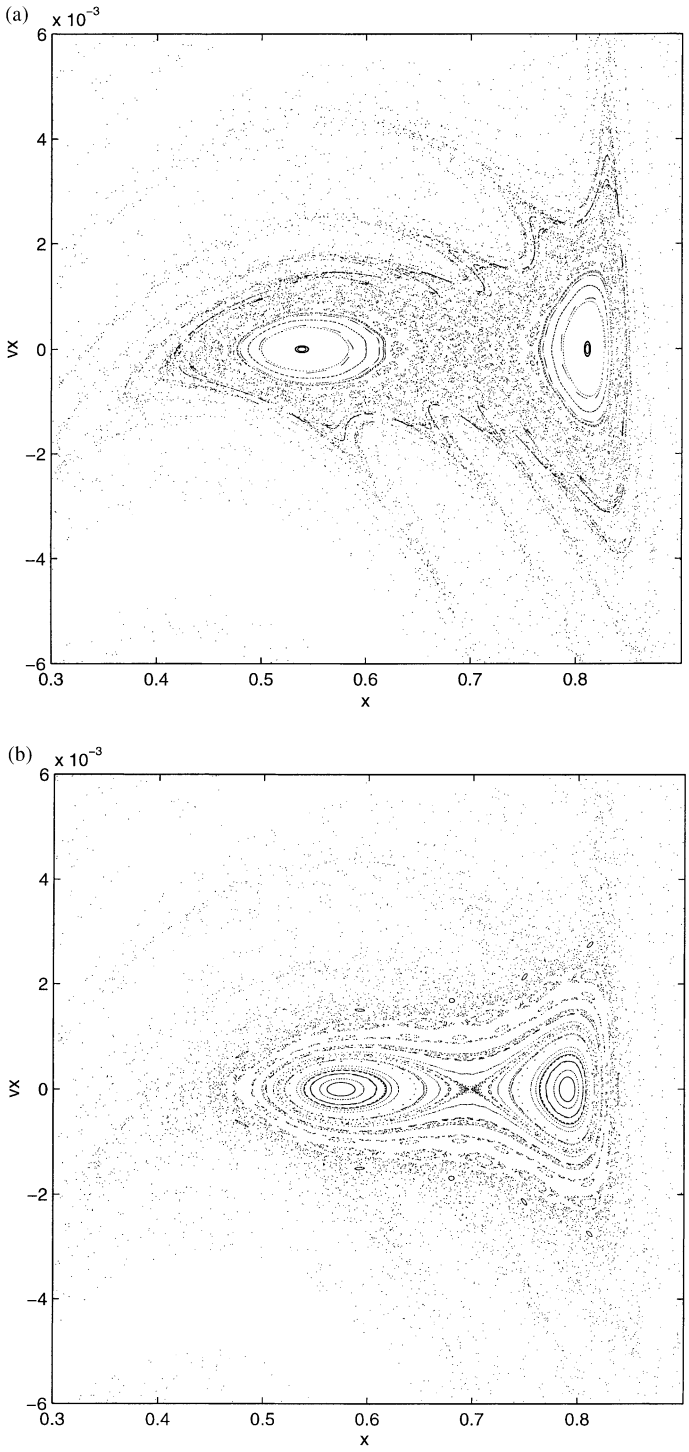

Fig. 3. SOS for B_y values near the observed bifurcation. It is observed that the KAM surfaces bifurcate in moving from $b_2 = 0.189$ to $b_2 = 0.188$. The trajectories shown in Fig. 5(c) and (d) correspond to the central KAM surface (i.e. the periodic orbit corresponding to stable fixed points in the x, v_x plane) in (c) and (d) above: (a) $b_2 = 0.186$; (b) $b_2 = 0.187$; (c) $b_2 = 0.188$; (d) $b_2 = 0.189$.

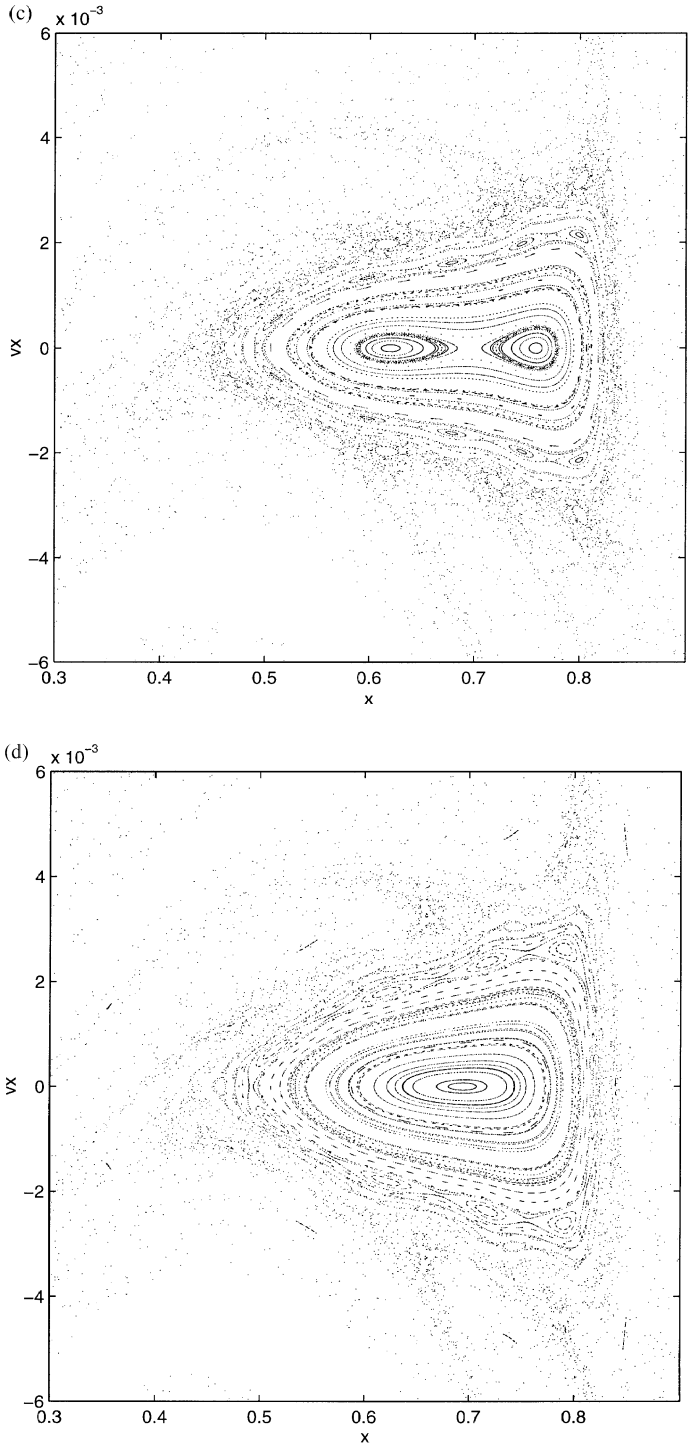

Fig. 3. (*Continued*).

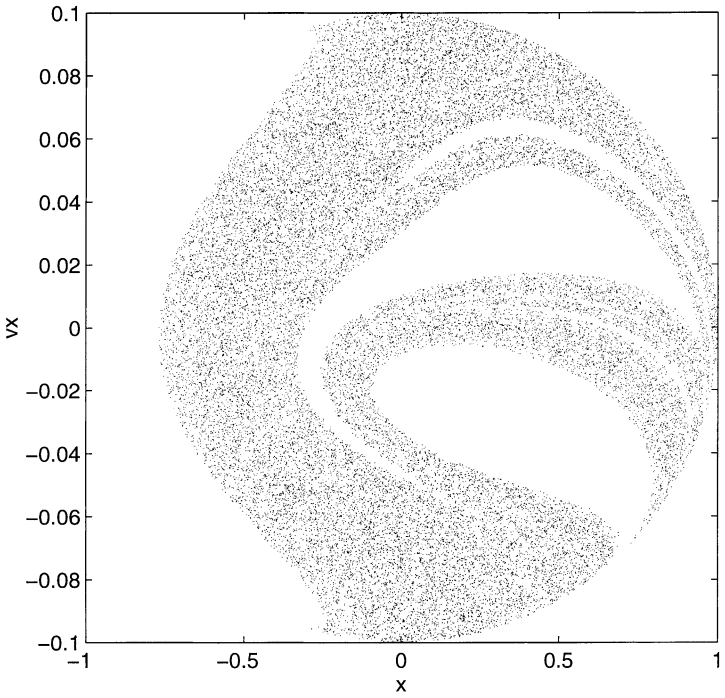

Fig. 4. SOS plot for $b_2 = 0.15$ demonstrating the absence of regular trajectories.

At $b_2 \approx 0.007$, a period 2 stable orbit then appears as a figure of eight trajectory, this is shown in Fig. 7. It should be noted that the effect of the small b_2 is to introduce a displacement along the x-axis between the two points where the orbits intersects the $z = 0$ plane. In the limit of vanishing b_2 the separation vanishes and the topology of the original figure of eight, see Fig. 1(a), is recovered. The stability of this type of orbit under small b_2 perturbations has been extensively discussed in [6].

5. Topology of KAM tori

In the previous section, period 2 orbits that are the centres of nested KAM surfaces on the SOS plots were discussed. When moving slightly away from these centers, by varying x, the orbits will be confined to KAM surfaces (tori in 3D). The trajectory shown in Fig. 8 is initiated at $x = 0.536481$ and corresponds to one of the KAM surfaces that are encompassing the bifurcated islands in Fig. 3(c) (only crossings of the $z = 0$ plane in one direction is used in the production of the SOS plots). The trajectory defines a surface in the shape of a Moebius strip. On closer inspection of the strip, it is found that the surface is a twisted and squashed torus (the SOS plots in Fig. 3 were indeed produced using a higher resolution of v_x coordinate to resolve the KAM surfaces corresponding to the squashed torus). The handedness of the strip is determined by the direction of the shear field and the squashing of one of the dimensions of the 3D-torus appear to be essential features of the imposed symmetry breaking; adding a b_2 component of opposite sign to the field will produce a Moebius strip of the opposite handedness.

The bifurcated Moebius strip shown in Fig. 9, and the corresponding detail, Fig. 9(b), for $x = 0.589$ corresponds to the two KAM surfaces around each of the islands in Fig. 3(c).

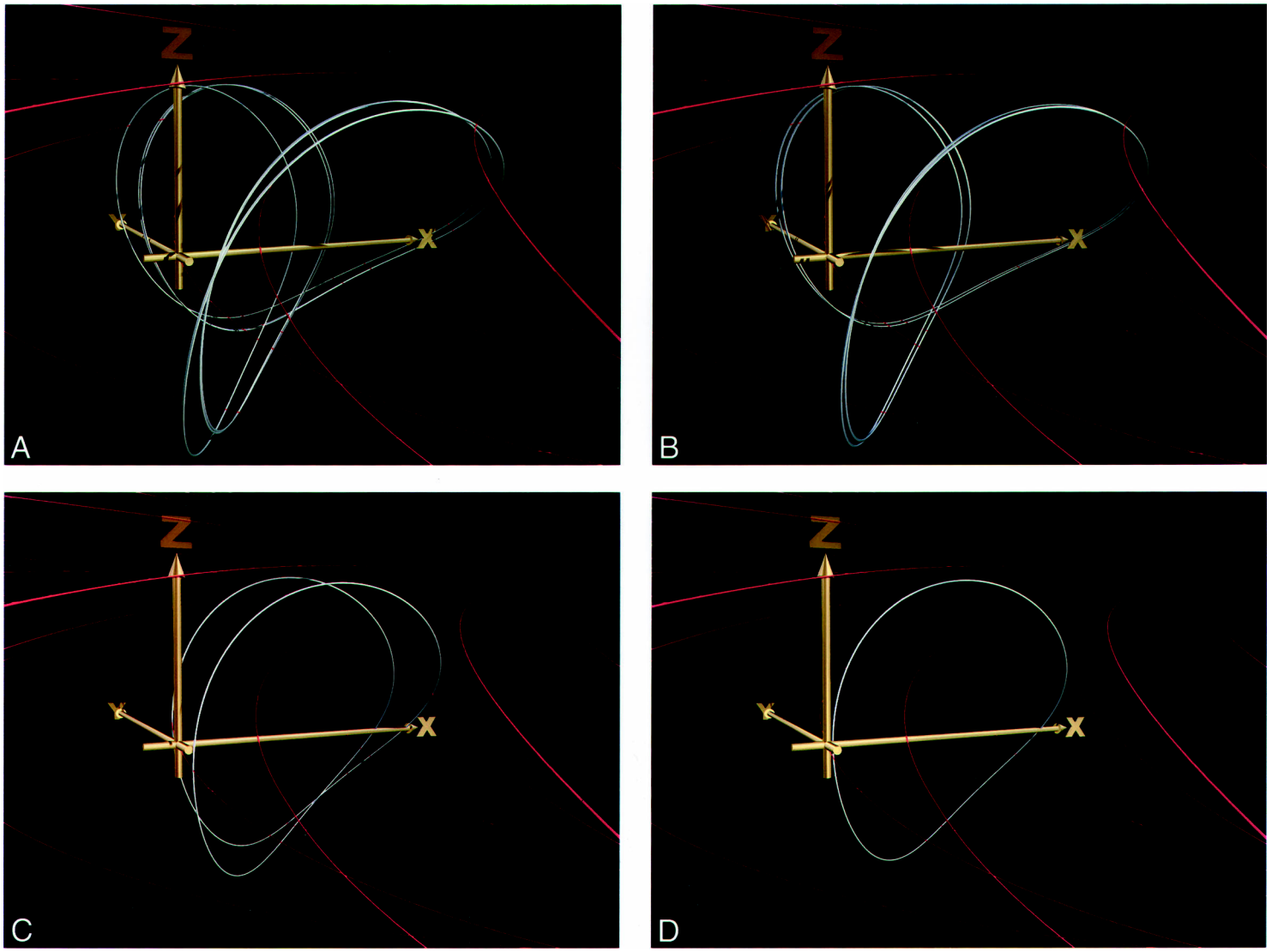

Fig. 5. Central periodic orbits near the observed bifurcations are shown in three-dimensional configuration space. The first bifurcation takes place when moving from $b_2 = 0.189$ to $b_2 = 0.188$. The starting point of each trajectory is given: (a) $b_2 = 0.1782$, $x = 0.41808$, $v_x = 0$; (b) $b_2 = 0.1790$, $x = 0.386$, $v_x = 0$; (c) $b_2 = 0.188$, $x = 0.620$, $v_x = 0$; (d) $b_2 = 0.189$, $x = 0.677$, $v_x = 0$.

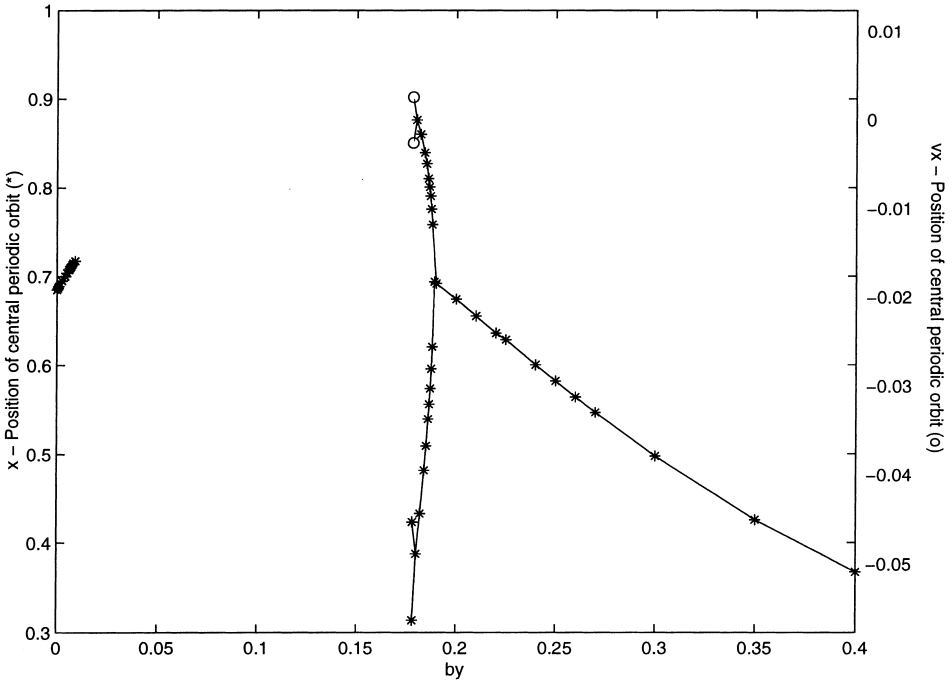

Fig. 6. The location of the central orbits at the *xy*-crossing as a function of b_2. The bifurcation at $b_2 \approx 0.188$ is the first in a series of bifurcations leading to chaos. It should be noted that successive bifurcations occur in Δx (marked with "$*$"), and Δv_x (marked with "0"). No stable periodic orbits are found in the region between $b_2 \approx 0.175$ and $b_2 \approx 0.007$.

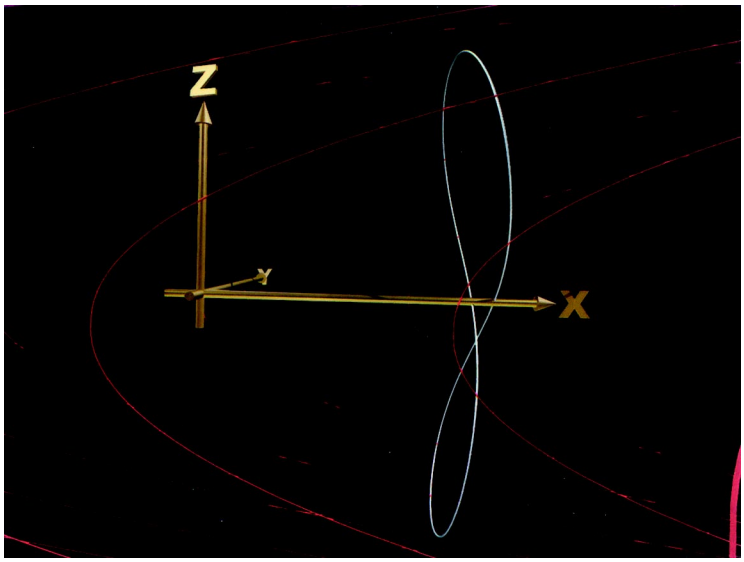

Fig. 7. The figure of eight orbit in three-dimensional configuration space is shown for $b_2 = 0.007$. The separation of the trajectory at the *xy* crossing is caused by the small symmetry breaking b_2 component.

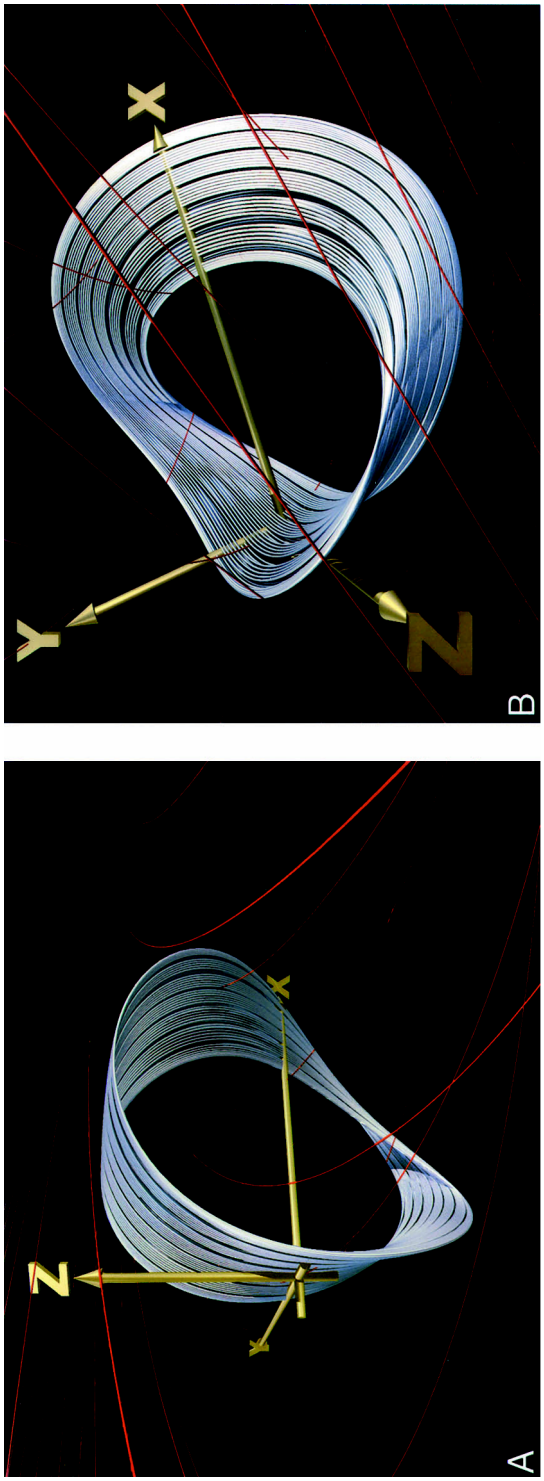

Fig. 8. (a) Regular orbit in three-dimensional configuration space in the shape of a Moebius strip showing the symmetry breaking handedness of the system. This trajectory corresponds to a KAM surface encompassing the bifurcated islands in Fig. 3(c) for $b_2 = 0.188$ and $x = 0.536$. In (b) a detail, from altered viewpoint, of the same trajectory is shown.

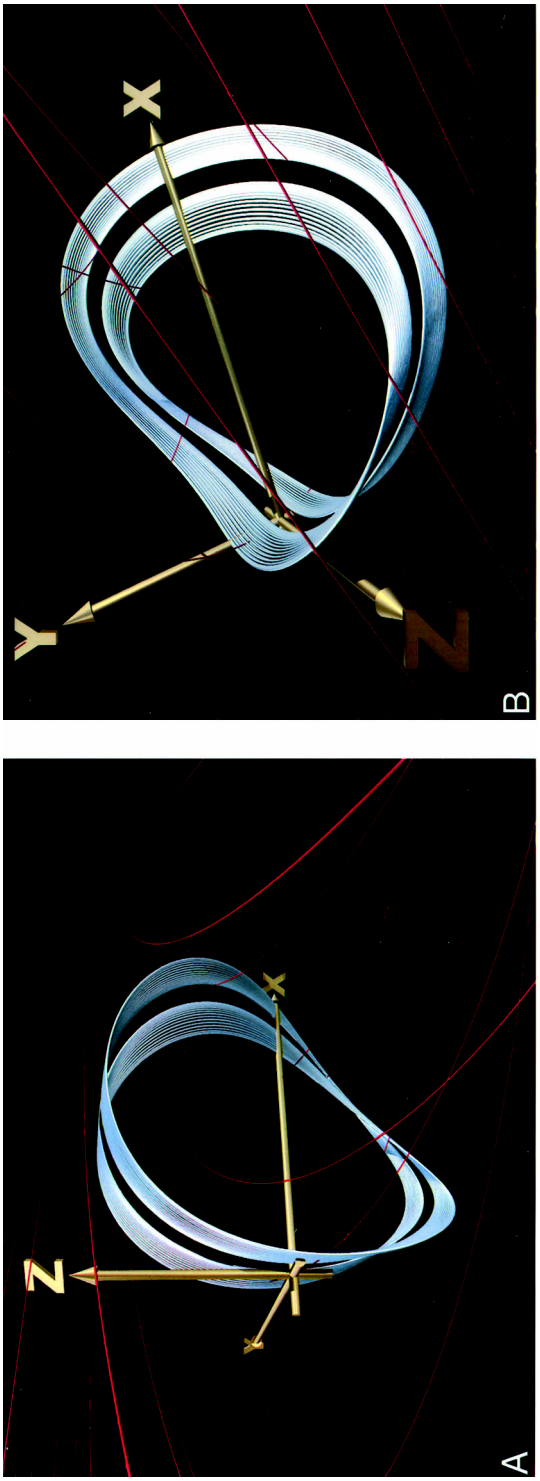

Fig. 9. (a) Regular orbit in three-dimensional configuration space in the shape of a bifurcated Moebius strip, indicating the first step towards the chaotic region. This trajectory corresponds to the two KAM surfaces encompassing the bifurcated islands in Fig. 3(c) for $h_2 = 0.188$ and $x = 0.589$. In (b) a detail, from altered viewpoint, of the same trajectory is shown.

6. Conclusion

By using 3D graphics in combination with SOS plots the phase space properties of a magnetic field reversal have been explored. The topological connection between the orbits in the integrable limit of large shear field and the periodic orbits near $b_2 = 0$ has been established. The bifurcation sequence leading to chaos for intermediate strengths of the shear field has been identified. Furthermore, plots of KAM tori in 3D are used to reveal the symmetry breaking features of the added shear field as a handedness of twisted phase space tori.

The interplay of 3D trajectories and SOS plots have played an instrumental role in the present effort to understand the properties of the studied system. It is thus obvious that the 3D trajectories together with the corresponding SOS plots constitutes a valuable tool in the exploration of phase space and corresponding topological structures. It should be noted that the topological features presented here were discovered initially by means of a semi-immersive Virtual Reality implementation of the 3D plotting algorithm.

References

[1] S.C. Baek, D.I. Choi, Dawn-dusk magnetic field effects on ions accelerated in the current sheet, J. Geophys. Res. 100 (1995) 14935.
[2] W. Baumjohann, R.A. Treumann, Basic Space Plasma Physics, Imperial College Press, 1997.
[3] J. Buchner, L.M. Zelenyi, Regular and chaotic charged particle motion in magnetotaillike field reversals. 1. Basic theory of trapped motion, J. Geophys. Res. 94 (1989) 11821.
[4] J. Buchner, L.M. Zelenyi, Regular and chaotic motion in sheared magnetic field reversals, Adv. Space Res. (1991) 11.
[5] S.C. Chapman, Properties of single particle dynamics in a parabolic magnetic reversal with general time dependence, J. Geophys. Res. 99 (1994) 5977.
[6] S.C. Chapman, G. Rowlands, Are particles detrapped by constant by instatic magnetic reversals?, J. Geophys. Res. 103 (1998) 4597.
[7] S.C. Chapman, N.W. Watkins, Parameterization of chaotic particle dynamics in a simple time-dependent field reversal, J. Geophys. Res. 98 (1993) 165–177.
[8] J. Chen, Nonlinear dynamics of charged particles in the magnetotail, J. Geophys. Res. 97 (1992) 15011.
[9] C. Goodrich, J.D. Scudder, J. Geophys. Res. 89 (1984) 6654.
[10] F.de Hoffman, E. Teller, Magneto-hydrodynamics shocks, Phys. Rev. 80 (1950) 697.
[11] H. Karimabadi, P.L. Pritchett, F.V. Coroniti, Particle orbits on two-dimensional equilibrium models for the magnetotail, J. Geophys. Res. 95 (1990) 17153.
[12] Y. Litvenko, App. J. 462 (1996) 997.
[13] V.A. Sergeev, D.G. Mitchell, C.T. Russell, D.J. Williams, Structure of the tail plasma/current sheet at $\sim 11r_e$ and its changes in the course of a substorm, J. Geophys. Res. 98 (1993) 17345.
[14] L.F. Shampine, M.K. Gordon, Computer Solution of Oridinary Differential Equations: The Initial Value Problem, Freeman, New York, 1990.
[15] Z.-D. Wang, Single particle dynamics of the parabolic field model, J. Geophys. Res. 99 (1994) 5949.
[16] Z. Zhu, G. Parks, Particle orbits in model current sheets with a nonzero b_y component, J. Geophys. Res. 98 (1993) 7603.